Terahertz spectroscopy of explosive materials

Yaochun Shen, Philip F. Taday, Michael C. Kemp*
TeraView Limited, Platinum Building, St Johns Innovation Park,
Cambridge CB4 0WS, United Kingdom

ABSTRACT

The terahertz spectrum of the explosive RDX has been measured using a conventional Fourier transform infrared spectroscopy and by terahertz pulse spectroscopy in transmission and reflection modes. Seven absorption features in the spectral range 5–120 cm^{-1} have been observed and identified as the fingerprints of RDX explosive. Furthermore, a sample consisting of RDX-based explosive, mounted side by side with lactose and sucrose pellets, has been imaged using a terahertz pulse imaging system. The recorded terahertz images and their spectral data have a spectral resolution of 1 cm^{-1} and cover a spectral range of 5–80 cm^{-1}. This broad spectral coverage enables the spatial distribution of individual chemical substances of the sample to be mapped out. We also discuss the application of Principal Component Analysis and Component Spatial Pattern Analysis to the automatic identification of materials, such as explosives, from terahertz imaging.

Keywords: terahertz pulsed imaging, terahertz spectroscopy, security screening, explosives detection, spectroscopic imaging, chemical mapping, principal component analysis, component spatial pattern analysis

1. INTRODUCTION

Terahertz imaging and spectroscopy has been identified as a very promising new technique for the detection of explosives and other threats in security screening at airports and elsewhere. The terahertz region of the electromagnetic spectrum (300GHz – 10 THz) has an unique combination of properties in that terahertz waves propagates through barrier materials such as clothing and packaging; many substances show characteristic spectral features in the terahertz; and, the radiation is non-ionising and does not give rise to safety concerns. At higher frequencies above a few terahertz into the infra red where there are even richer spectroscopic features, absorption and scattering limits penetration through barrier materials. At lower frequencies, such as the millimetre waves below say 300GHz there are no characteristic vibrational modes in solids leading to featureless spectra which cannot be used for identification.

In an earlier paper Kemp et al[1] reported measurements showing spectral features in a number of common energetic substances including 1,3,5-trinitro-1,3,5-triazacyclohexane (RDX), tetranitro-tetracyclooctane (HMX), pentaerythritol (PETN), trinitrotoluene (TNT) and also showed that commercial explosives based on these materials such as PE-4 and Semtex show the spectral features of their constituent explosives. Subsequently, measurements by other groups[2-4] have validated these results and, below, we report measurements carried out by several different techniques and on different samples – providing further validation.

Despite the high sensitivity and dynamic range of the terahertz pulsed spectroscopy technique we use, crystalline materials such as RDX have a very high absorption coefficient and any practical implementation of a security system will need to use reflection rather than transmission geometry. Here, we report what we believe to be the first experimental reflection spectroscopy measurements of terahertz spectra from explosives and show that the features we observe, match those predicted from transmission measurements.

Practical security systems will also require automated methods of identifying threat materials from their spectral features, both for reasons of operational convenience and speed, and, to enable use by operators who are not trained spectroscopists. Automatic pattern matching techniques and classifiers can be employed. Here, we discuss the use of Principal Component Analysis as a classification technique and again present data showing the method in use.

* mike.kemp@teraview.com; phone: 44 1223 435380; fax: 44 1223 435382; www.teraview.com

Passive Millimetre-Wave and Terahertz Imaging and Technology, edited by
Roger Appleby, J. Martyn Chamberlain, Keith A. Krapels, Proceedings of SPIE Vol. 5619
(SPIE, Bellingham, WA, 2004) · 0277-786X/04/$15 · doi: 10.1117/12.577188

2. MATERIALS AND METHOD

α–Lactose monohydrate and sucrose (Sigma-Aldrich, UK) were studied. The lactose was milled to a fine powder (particle size <100 μm). The sucrose was used in the original granulated form (particle size ~ 500 μm). Lactose powder and sucrose were compressed under 2-tons using a hydraulic press (Specac, UK) to form circular pellets together with high-density polyethylene (PE, particle size < 80 μm, Chesham Chemicals, UK). The PE powder acts as a pellet binder and is spectroscopically inert. Two pellets were prepared - pure lactose and pure sucrose. These two pellets, together with a small piece of RDX- based sheet explosive a few millimetres square were mounted at the terahertz focus position for reflection measurements. For transmission measurements, 30 mg sugar or explosive sample was first diluted/mixed with 300 mg PE powder, and then mixture was compressed to form pellet.

A *TPI™spectra 1000* (TeraView Ltd, Cambridge, UK), was used to record the transmission spectrum of powdered RDX in a PE matrix in the spectral range 5–120 cm^{-1}. For comparison, we also used a *Bruker IFS113V FTIR spectrometer* equipped with a 6 μm Mylar beam-splitter, and a liquid-Helium-cooled silicon bolometer. For all reflection measurements, we used a *TPI™scan* imaging system (TeraView Ltd, Cambridge, UK), operating at a rapid scan mode. In the experiment, the terahertz radiation reflected from a sample was measured in time domain over a scan range of about 5 mm, providing a spectral resolution of 1 cm^{-1} in spectral range 5–80 cm^{-1}. Terahertz spectral images were obtained by raster scanning the terahertz beam across the sample. The scanned area was 8 mm × 24 mm, which corresponds to 80 × 240 pixels at 100 μm spacing. We will show in the next section that these time-domain terahertz images contain all necessary information for mapping out the spatial distribution of chemical components of a sample.

3. RESULTS AND DISCUSSIONS

3.1 Transmission spectra

To validate that THz technology can be used for detecting explosives, we first measured the absorption spectrum of RDX using a transmission THz spectrometer, i.e., *TPI™spectra 1000*. In TPS measurement, the electric field, instead of the intensity, of the THz radiations are measured. The electric field of the transmitted THz radiation can be described as:

$$T(\nu) \equiv E_t(\nu) / E_0(\nu) = e^{-\alpha(\nu)d}\, e^{j2\pi\nu d\, n(\nu)/c}$$

It has been shown[5-10] that both absorption coefficient ($a(\nu)$) and refractive index ($n(\nu)$) can be calculated from a single measurement, because the electric field measurements provide both amplitude and phase information. Furthermore, the absorption coefficient (at absorption peak) of most materials is a few tens of cm-1 and the sample thickness is a few millimetres. At absorption peaks, the transmittance drops significantly from 100% to a few percent. Therefore the transmission measurement is very sensitive to absorption features of the sample.

Figure 1(a) shows the amplitude of the Fourier transform of the THz waveform measured in the presence of a PE pellet (curve 1 of Figure 1(a)) and the RDX pellet (curve 2 of Figure 1 (a)). It is clear that the FFT amplitude of the measured THz signal after propagating through the RDX pellet decreases dramatically owing the strong absorption of RDX. The absorption spectrum of RDX was then calculated using a PE pellet as a reference. As shown in Figure 1(b), seven absorption features centred at 27.2, 34.9, 46.0, 51.8, 65.5, 74.2, 105.5 cm^{-1} were found in the spectral range 5–120 cm^{-1}. We note that the THz absorption spectrum of RDX was first reported by Kemp et al[1] and was subsequently confirmed by Yamamoto et al[2]. Our latest results reported in this paper agree very well with previous results[1-3] but with extended spectral coverage.

To verify that the spectral features observed using THz spectrometer are specific to RDX explosive, the same RDX sample was further examined using a Bruker IFS113V FTIR spectrometer equipped a liquid-Helium-cooled silicon bolometer. The measured transmission spectra agree very well, as shown in Figure 1(b).

3.2 Reflection spectra

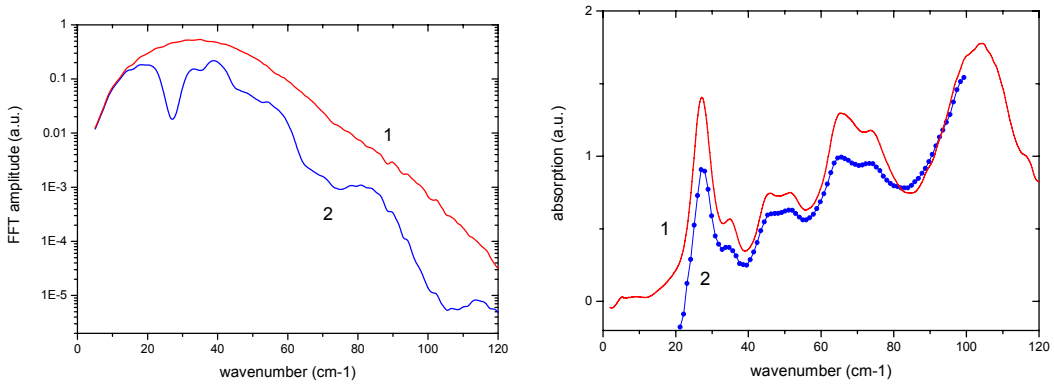

Figure 1 (a): Fourier transform amplitude of the measured THz waveform after transmitting through a PE pellet (curve 1) and a RDX pellet (curve 2). (b): absorption spectrum of RDX pellet measured using a THz spectrometer (curve 1) and a FTIR spectrometer (curve 2).

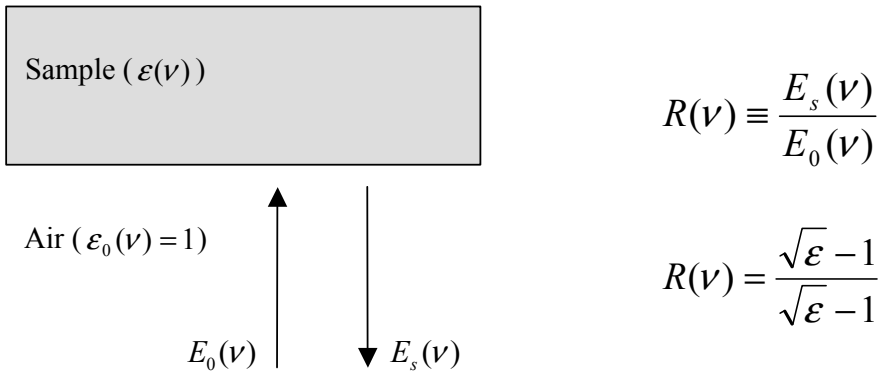

Figure 2: The reflection of THz radiation at air/sample interface and related equations.

In the previous section we have shown that reliable absorption spectra can be obtained using either FTIR or THz spectrometer operating at transmission mode. For some practical applications such as security screening, reflection measurement is necessary due to the high absorption coefficients of explosives. In this section we will show that the absorption spectra can be extracted from TPS reflection measurements. Figure 2 shows schematic representation of THz reflection at air/sample interface and the related equations for calculating its reflectance. At THz frequency range, the complex refractive index $\sqrt{\varepsilon(\nu)}$ for most samples can be written as: $\sqrt{\varepsilon(\nu)} = n(\nu) + j\alpha(\nu)c/2\pi\nu \approx n(\nu)$.

Therefore, unlike transmission spectrum which is dominated by the absorption coefficient $\alpha(\nu)$ of the sample, the reflection spectrum mostly reflects the refractive index $n(\nu)$ of the sample. Figure 2 (a) shows the FFT amplitude of the THz waveform measured after reflecting from a PE pellet and from a piece of RDX explosive. As expected, the FFT amplitude in reflection measurement (curve 2 of Figure 3(a)) is remarkably different from its counterpart in transmission measurement (curve 2 of Figure 1 (a)). However, the absorption coefficient and the refractive index of the sample can still be extracted from the reflection measurement.

For this purpose, we assume that $E_S(\nu)$ and $E_M(\nu)$ are the Fourier transform of the measured THz waveform reflected from a sample and a reference mirror. The absorption coefficient, $\alpha(\nu)$, and the refractive index, $n(\nu)$, are calculated as:

$$\sqrt{\varepsilon} \equiv n(\nu) + j\frac{\alpha(\nu)c}{4\pi\nu} = \frac{1-R(\nu)}{1+R(\nu)}$$

where $R(\nu) \equiv E_s(\nu)/E_M(\nu)$. It is worthwhile to note that in real measurement, the sample and the reference may not be in the exact same position. Therefore the true reflectance will take form as: $R'(\nu) = R(\nu)\, e^{jk(\nu)2\Delta x}$. Here Δx is the position difference between reference and sample measurements. This clearly will introduce additional imaginary component in the equation and thus give serious problems when calculating absorption coefficient. One approach to extract absorption coefficient of the sample is to purposely introduce a phase shift ($e^{-jk(\nu)2\Delta x}$) in the calculated reflectance before calculating the absorption coefficient. This compensates the phase shift caused by the imperfection in the measurement such as the rough surface of the sample. As shown in Figure 3(b), the absorption coefficient extracted from both transmission and reflection measurement has essentially the same spectral features. Similar results have also been obtained for pure lactose and sucrose pellets (Figure 4). Therefore we can conclude that the first derivative spectra measured in reflection mode (curves labelled '1') are the same as those measured in typical transmission measurements (curves labelled '2'). We believe these results represent the first *measured* THz reflection spectrum for RDX, and note that they agree well with the calculated THz reflection spectrum of RDX derived by Yamamoto et al[2] from their transmission measurements.

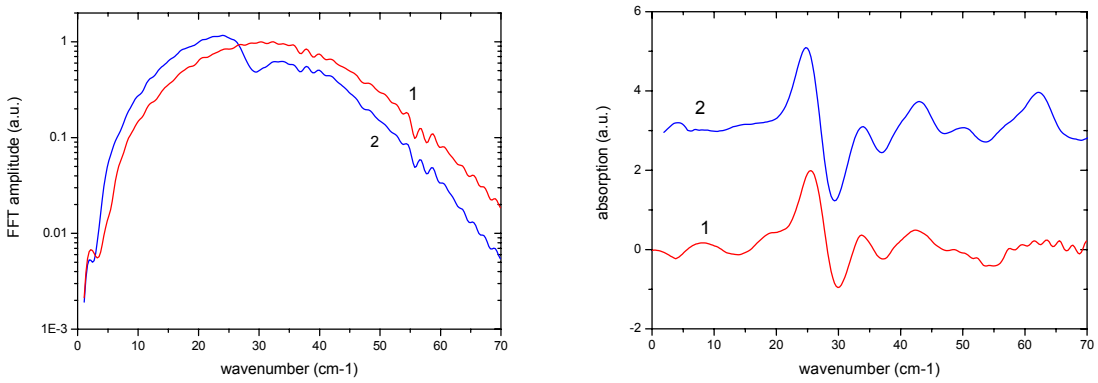

Figure 3 (a): Fourier transform amplitude of the measured THz waveforms after reflecting from a PE pellet (curve 1) and a RDX pellet (curve 2). (b): the first derivative absorption spectrum of RDX pellet obtained from a reflection measurement (curve 1) and a transmission measurement (curve 2).

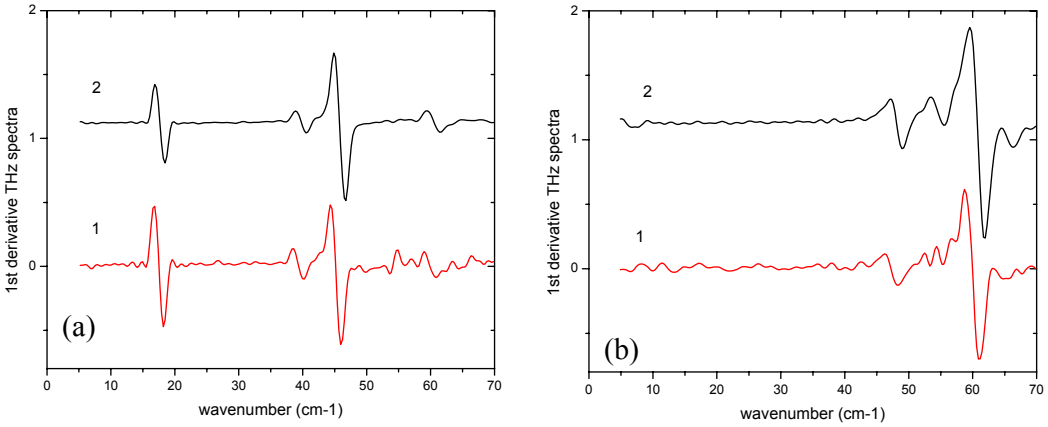

Figure 4 The first derivative spectra of the absorption coefficient of lactose (a) and sucrose (b). Curve 1: spectrum derived from terahertz reflection measurement; curve 2: spectrum derived from terahertz transmission measurement.

3.3 Chemical mapping using component spatial pattern analysis

Figure 5(a) shows the time-domain THz image which is generated by using the peak amplitude of the measured THz waveforms. We saw a uniform image in lactose area whist we saw some contrast in sucrose area owing to the relative large sucrose particles presented in sucrose pellet. Unlike lactose and sucrose pellet whose surface is relative smooth, the piece of sheet explosive (used as supplied) has a larger surface roughness giving rise to more contrast as shown in Figure 5(a). However, from the time-domain THz image alone we can not tell if a specific area is lactose, sucrose or explosives.

For the purpose of detecting and identifying explosives, we first Fourier transformed the time-domain THz waveform, and then calculated the absorption spectrum for each pixel of the image, each in the same manner as discussed in previous sections. This generated a three-dimensional data set where two axes describe vertical and horizontal spatial dimensions, and the third axis represents the spectral frequency dimension. In order to extract the spatial distributions of individual chemical substances in the sample, we first compress the three-dimensional data set to a two-dimensional matrix F_{NxL}, which has L pixels each with N frequency components. If we assume that the sample has M chemical substances (M = 3 for the present case) and each chemical substance has a known absorption spectrum with N frequency components, we then have a matrix of S_{NxM}. The spatial distribution of individual chemical substances in the sample is then calculated using the Component Pattern Analysis method[11] as:

$$[P_{MxL}] = ([S_{NxM}]^t[S_{NxM}])^{-1}[S_{NxM}]^t[F_{NxL}]$$

where P_{ij} represents the probability of the occurrence of the *i-th* substance (i = 1 for lactose, i = 2 for sucrose, and , i = 3 for RDX) at the *j-th* pixel (j = 1, 2, …, L, and L = 80x240). Note that the spectral matrix S_{NxM}, which forms the basis for chemical mapping analysis, can be obtained from either reflection or transmission THz measurements.

Figure 5 (b)–(c) shows the chemical mapping THz images reconstructed using $P_{1j}(j = 1,2,...,L)$ As expected, P_{1j} has large values across the entire lactose pellet (left of Figure 4(b)), whist P_{1j} is close to zero across most of the sucrose pellet (middle of Figure 5 (b)) and RDX explosives (right of Figure 4 (b)). The reverse is also true for the THz image shown in Figure 5(c) and (d), which is constructed using P_{2j} and P_{3j}, respectively (j = 1, 2, …, L) and thus corresponds to spatial distribution of sucrose and RDX.

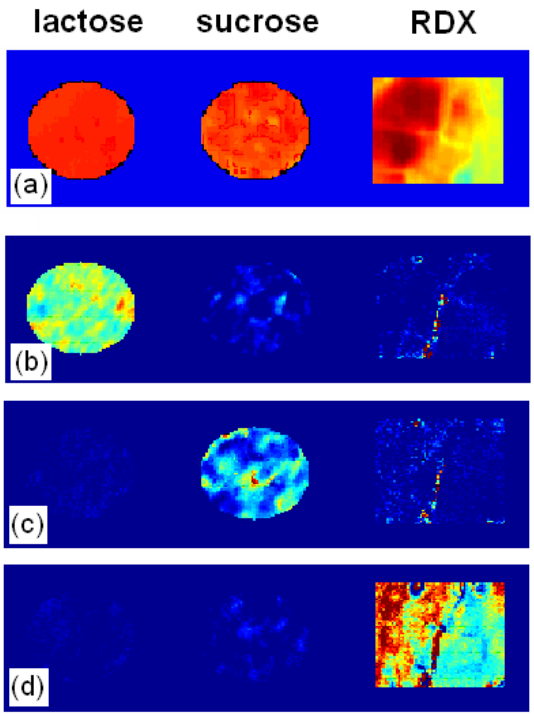

Figure 5 False-colour terahertz chemical mapping images showing the spatial distributions of lactose (b), sucrose (c) and RDX (d). The THz time-domain image (peak amplitude) is shown in (a).

For practical security screening applications, we can construct a spectral matrix S_{NxM} comprising THz spectra of known explosives. We can apply this spectral matrix to THz images measured for a suspicious subject. Any bright spot/area in the reconstructed chemical map may indicate the possible presence of explosive. For example, after applying the THz spectrum of RDX to analysing the THz spectroscopic images, only area containing RDX is highlighted (see Figure 4(d)) demonstrating that TPI has the sensitivity and specificity for detecting and identifying explosives such as RDX. We note that these techniques can be used for other detection and chemical mapping applications such as the detection of illicit drugs using spectral fingerprints[11].

3.4 Principal component analysis

The spectroscopic THz images obtained with a TPI system contain comprehensive information on both spatial and chemical distribution of the sample. In the previous sections, we demonstrated that the chemical distribution at the sample surface can be mapped out by using the known spectral features of a given chemical. In this section, we will show that the principal spectral features of an unknown sample can be extracted from the spectroscopic THz images by using principal component analysis (PCA). PCA is a classical technique to reduce the dimensionality of the data set by transforming to a new set of variables (the principal components) to summarize the features of the data[12]. Principal components are uncorrelated (orthogonal) and ordered such that the *k*-th component has the *k*-th largest variance among all components. There are two possible applications of PCA to THz image analysis: the first is to extract/summarize the similarity of the spectral features for all pixels of THz images, and the second is to extract/summarize the common spatial features of a set of THz images (facial recognition in the context of computer vision). In the rest of this section we will discuss the first application of PCA to THz image analysis.

Assume that we have L column vectors ($P_1, P_2, ..., P_L$), each has N frequency components and represents a THz spectrum at a pixel of the sample. For PCA to work properly, it is better to subtract the mean from the data dimensions. This produces a new vector data set ($W_1, W_2, ..., W_L$) whose mean is zero: $W_k = P_k - \frac{1}{L}\sum_{k=1}^{L} P_k$. The goal of PCA, in the present context, is to determine from the set of W_k 's a basis for the subspace (principal components) within which most of the images can be represented with a small amount of error. Mathematically, we can express this goal as to find a set of M orthogonal vectors V_k for which the quantity $\lambda_k = \frac{1}{L}\sum_{n=1}^{L}(V_k^t W_n)^2$ is maximized, subject to the orthogonal constrain: $V_l^t V_k = \delta_{lk}$. Using Rayleigh's principle, it can be shown that V_k and λ_k are given by the eigenvectors and eigenvalues of the covariance matrix:

$$[C_{NxN}] = [W_{NxL}][W_{NxL}]^t$$

where $[W_{NxL}]$ is a matrix comprised of the column vectors W_k placed side by side. The covariance matrix $[C_{NxN}]$ has N eigenvectors and N eigenvalues. In general, once eigenvectors are found from the covariance matrix, the next step is to order them by eigenvalue, highest to lowest. This gives you the components in order of significance. As example, Figure 6(a) shows the first 6 of 256 principal components extracted from the THz spectroscopic images of a lactose pellet. In this case, the first principal component extracted, which account for 73% of the variance of the data set, is close to the

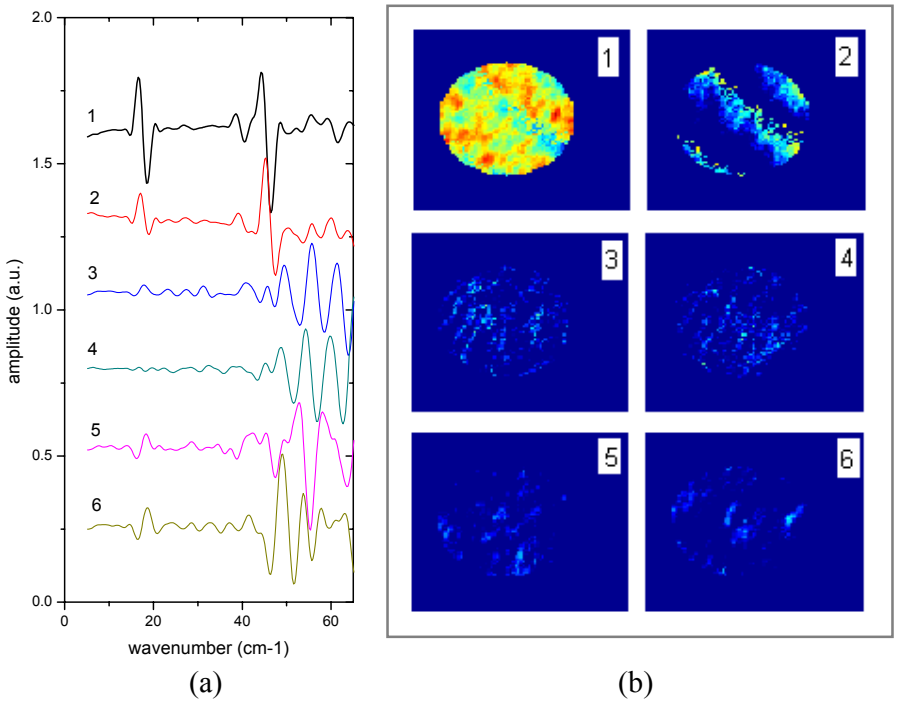

Figure 6 (a) The first six principal components extracted from the THz spectroscopic images of a lactose pellet. Curve 1 is the first principal component. The eigenvalues of these six eigenvectors (principal components) are 73%, 10%, 2.8%, 2.2%, 1.8% and 1.5%, respectively. (b) THz images reconstructed using these six principal components.

first derivative of the absorption spectrum of lactose (Figure 3 (a)). The first 6 principal components in total account for over 90% variance in the data. Therefore one can reduce the dimensionality of the data set from initial 256 to 6 without losing much of the information. This is very useful for detecting and identifying explosives in real time where the data size of the THz spectroscopic images may be a big issue. In addition, PCA is also useful to extract the spectral information for unknown samples. The extracted spectral information can be further used in the chemical mapping process discussed in section 3.3.

4. CONCLUSIONS

In this paper we have demonstrated the capability of TPI for detecting and identifying the explosives and for chemical mapping the spatial distribution of individual chemical substances in a sample. Our result reported here is the first THz chemical mapping of explosives realised using reflection THz measurements and represents, we believe, a significant advance towards developing a TPI system for security screening of explosives. In addition, the TPI spectroscopic images reported here cover a broad spectral range of 5–80 cm^{-1} enabling us precisely to map out the spatial distribution of the individual chemical substances in a sample in a single measurement.

ACKNOWLEDGEMENTS:

Parts of this work were carried out under contract for the UK Government whose support is gratefully acknowledged. The authors thank T. Lo for FTIR spectroscopy measurements on RDX.

REFERENCES:

1. M.C. Kemp, P.F. Taday, B.E. Cole, J.A. Cluff, A.J. Fitzgerald and W.R. Tribe, *SPIE 5070*, 44 (2003)
2. K. Yamamoto et al., Japn. J. Appl. Phys. 43, L414 (2004)
3. W.R. Tribe, D.A. Newnham, P.F. Taday and M.C. Kemp, *SPIE 5354*, 168 (2004)
4. D.J. Cook, B.K. Decker, G.Maislin and M.G. Allen, *SPIE 5354*, 55 (2004)
5. T.D. Dorney, R.G. Baraniuk, and D.M. Mittleman, *J. Opt. Soc. Am. A* 18, 1562 (2001).
6. B. Ferguson and X.-C. Zhang, *Nat. Mater.* 1, 26 (2002)
7. M.C. Beard, G.M. Turner, and C. A. Schmuttenmaer, *J. Phys. Chem. B* 106, 7146 (2002)
8. (a) M. Walther, B. Fischer, M. Schall, H. Helm, and P. Uhd Jepsen, *Chem. Phys. Lett.* 332, 389 (2000); M. Walther, B.M. Fischer and P. Uhd Jepsen, *Chem. Phys.* 288, 261 (2003)
9. (a) Y.C. Shen, P.C. Upadhya, A.G. Davies & E.H. Linfield, *Appl. Phys. Lett.* 82, 2350 (2003); Y.C. Shen, P.C. Upadhya, E.H. Linfield, and A.G. Davies, *Vib. Spectrosc.* 35, 111 (2004)
10. (a) P.F. Taday, I.V. Bradley, D.D. Arnone, and M. Pepper, *J. Pharmaceutical Sci*. 92, 831-838 (2003). (b) C.J. Strachan, T. Rades, D.A. Newnham, K.C. Gordon, M. Pepper, and P.F. Taday, *Chem. Phys. Lett.* **390**, 20 (2004*)*. (c) A.J. Fitzgerald, B.E.Cole and P.F. Taday, *J. Pharmaceutical Sci*. in press (2004)
11. Y. Watanabe, K. Kawase, T. Ikari, H. Ito, Y. Ishikawa and H. Minamide, *Appl. Phys. Lett.* 83, 800 (2003)
12. I.T. Jolliffe, Principal Component Analysis, (Springer, New York, 1986)